






Strong lateral exchange coupling and current-induced switching in single-layer ferrimagnetic films with patterned compensation temperature

Zhentao Liu ^{1,2}, Zhaochu Luo ^{1,2,3,4,*}, Ivan Shorubalko ⁵, Christof Vockenhuber,⁶ Laura J. Heyderman ^{1,2}, Pietro Gambardella ^{7,†} and Aleš Hrabec^{1,2,7,‡}

¹Laboratory for Mesoscopic Systems, Department of Materials, ETH Zurich, 8093 Zurich, Switzerland

²Laboratory for Multiscale Materials Experiments, Paul Scherrer Institute, 5232 Villigen PSI, Switzerland

³State Key Laboratory for Mesoscopic Physics, School of Physics, Peking University, 100871 Beijing, People's Republic of China

⁴Beijing Key Laboratory for Magnetoelectric Materials and Devices, 100871 Beijing, People's Republic of China

⁵Transport at Nanoscale Interfaces Laboratory, Empa - Swiss Federal Laboratories for Materials Science and Technology, 8600 Dübendorf, Switzerland

⁶Laboratory of Ion Beam Physics, ETH Zürich, 8093 Zürich, Switzerland

⁷Laboratory for Magnetism and Interface Physics, Department of Materials, ETH Zurich, 8093 Zurich, Switzerland



(Received 15 July 2022; revised 27 January 2023; accepted 27 February 2023; published 20 March 2023)

Strong, adjustable magnetic couplings are of great importance to all devices based on magnetic materials. Controlling the coupling between adjacent regions of a single magnetic layer, however, is challenging. In this work, we demonstrate strong exchange-based coupling between arbitrarily shaped regions of a single ferrimagnetic layer. This is achieved by spatially patterning the compensation temperature of the ferrimagnet by either oxidation or He⁺ irradiation. The coupling originates at the lateral interface between regions with different compensation temperature and scales inversely with their width. We show that this coupling generates large lateral exchange coupling fields and we demonstrate its application to control the switching of magnetically compensated dots with an electric current.

DOI: [10.1103/PhysRevB.107.L100412](https://doi.org/10.1103/PhysRevB.107.L100412)

In spintronic architectures based on magnetic multilayers [1–3], interlayer couplings such as the Ruderman-Kittel-Kasuya-Yosida interaction [4,5], exchange coupling leading to exchange bias [6,7] and the dipolar interaction [8–10] allow for the tuning of the magnetic stability and electrical properties of the device [1–3]. The exchange interaction, composed of symmetric and antisymmetric parts, provides the strongest coupling channel in magnetic systems. The symmetric part favors collinear magnetic configurations and is commonly exploited in multilayers to provide direct exchange coupling between, for example, two ferromagnets [11] or a ferromagnet and an antiferromagnet [6], and indirect coupling between two ferromagnets separated by a nonmagnetic spacer [4,5]. The antisymmetric part, known as the Dzyaloshinskii-Moriya interaction (DMI), favors noncollinear magnetic textures, but is generally indirect and weaker in multilayer systems [12–14]. Controlling the coupling between adjacent regions of a single magnetic layer is more challenging [15–17]. In single layers, the interfacial DMI provides a means to couple planar structures [16,18], which has enabled the realization of electrically controlled magnetic logic devices [19–23]. However, the strength of this coupling is limited by the interface properties [24]. The stronger collinear exchange coupling in magnetic multilayers thus lacks a counterpart in the lateral direction.

In this work, we realize a strong lateral coupling based on the exchange interaction in a single magnetic layer. We take inspiration from an approach previously developed for synthetic ferrimagnetic systems consisting of stacked layers of rare-earth transition-metal ferrimagnets with different magnetic compensation temperature (T_M) [25–31]. This type of multilayer is also known as an exchange spring magnet and includes a compensation wall. We further develop this method, applying it to a single-layer ferrimagnetic alloy. In such an alloy, the strong intralattice coupling between the transition-metal atoms and the weaker interlattice coupling between the rare-earth and transition metal atoms can be separately tuned by altering the composition [32] or microstructure [33], and through reduction/oxidation reactions [34,35]. Recently, He⁺ irradiation has been used to modify T_M in a Co/Tb multilayer in order to create multidomain configurations with dimensions of several μm [30,36]. Here we show that patterning of T_M in a single GdCo film by either selective oxidation or He⁺ irradiation leads to strong lateral exchange coupling between regions with different T_M . We show how the coupling varies as a function of temperature and width of the patterned regions. We discuss the strength of the coupling and compare the exchange interaction in our planar structures with that found in multilayer systems. We further combine spin-orbit torques [3] and lateral coupling in a Pt|GdCo bilayer to demonstrate selective current-induced switching of adjacent magnetic domains, which results in reproducible manipulation of lateral exchange bias.

*zhaochu.luo@pku.edu.cn

†pietro.gambardella@mat.ethz.ch

‡ales.hrabec@psi.ch

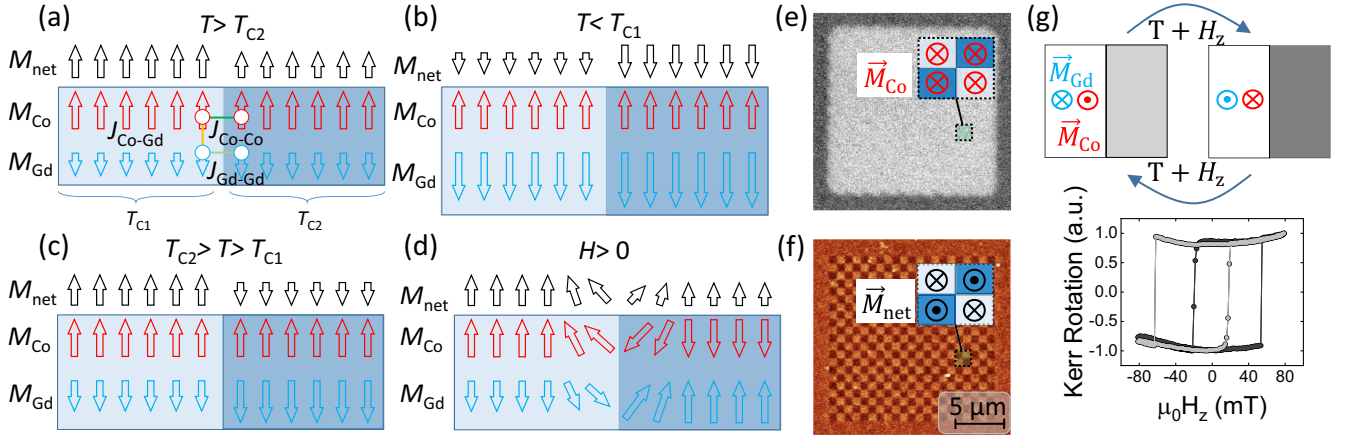


FIG. 1. Demonstration of the lateral exchange coupling principle. (a)–(d) Schematic of interfacial exchange coupling at different temperatures. $\mathbf{M}_{\text{net}} = \mathbf{M}_{\text{Co}} + \mathbf{M}_{\text{Gd}}$. The dark and light blue background correspond to the nonoxidized and oxidized regions, respectively. The $J_{\text{Co-Co}}$ (green), $J_{\text{Gd-Gd}}$ (light green), and $J_{\text{Co-Gd}}$ (yellow) represent exchange coupling between different elements, respectively. (e) Kerr image and (f) MFM image of the checkboard pattern spontaneously formed in 800-nm-wide GdCo squares at zero field. The symbols in the insets represent the orientation of the magnetization of the Co sublattice (red) and the net magnetization (black) while the dark and light blue background correspond to the nonoxidized and oxidized sections, respectively. (g) Hysteresis loops measured on a 50- $\mu\text{m} \times 50\text{-}\mu\text{m}$ GdCo square with one half being magnetically compensated (in white) and the other half being oxidized (in light or dark gray). The dark and light gray data points correspond to measurements taken after field cooling the sample from $T = 250$ to 300 K at -6 and $+6$ T (H_z), respectively.

Our Ta(1 nm)|Pt(5 nm)|Gd_{0.3}Co_{0.7}(x nm)|Ta(2 nm) multilayers possess out-of-plane (OOP) magnetization with x in the range 3.2–6.2 nm, where T_M can be tuned by changing the stoichiometric ratio or the thickness of the GdCo layer as shown in the Supplemental Material [37] (see, also, Ref. [38] therein). To spatially modify T_M , we use an oxygen plasma to partially oxidize the magnetic film in specific regions. The effect of oxidation is verified by Rutherford backscattering technique [37]. In particular, a GdCo film with $T_M = T_{c2}$ above room temperature (RT) can be oxidized in order to lower the compensation point below room temperature (T_{c1}). Magneto-optic Kerr effect (MOKE) measurements, which are predominantly sensitive to the magnetization of the Co sublattice, show a reversal in the hysteresis loop after oxidation of a GdCo film [37], indicating that T_M is suppressed below room temperature after the oxidation.

For a device containing two regions with different T_M ($T_{c2} > T_{c1}$), one can distinguish between three temperature scenarios illustrated in Figs. 1(a)–1(c): (i) the temperature is higher than both compensation temperatures ($T > T_{c2}$), (ii) the temperature is lower than both compensation temperatures ($T < T_{c1}$), and (iii) the temperature is lower than the compensation temperature of the original film but higher than the compensation temperature of the partially oxidized film ($T_{c2} > T > T_{c1}$).

In the temperature scenarios with $T > T_{c2}$ and $T < T_{c1}$ [Figs. 1(a) and 1(b)], all of the Co magnetic moments are parallel to each other and all of the Gd moments are antiparallel to the Co moments, minimizing the exchange and magnetic anisotropy energy. The net magnetization is then given by the sum of the two sublattice magnetizations, $\mathbf{M}_{\text{net}} = \mathbf{M}_{\text{Co}} + \mathbf{M}_{\text{Gd}}$. At a temperature $T > T_{c2}$ ($T < T_{c1}$), \mathbf{M}_{net} is parallel to \mathbf{M}_{Co} (\mathbf{M}_{Gd}) in both the pristine and oxidized regions of the film [Figs. 1(a) and 1(b)]. Because the neighboring Co moments are strongly exchange coupled and prefer to maintain a par-

allel alignment, not only within the two different regions but also across the interface between them, the net magnetization in the two regions is effectively (trivially) ferromagnetically coupled.

In the temperature range $T_{c2} > T > T_{c1}$, however, \mathbf{M}_{net} is parallel to \mathbf{M}_{Co} in the region with T_{c1} but parallel to \mathbf{M}_{Gd} in the region with T_{c2} . Hence, the low-energy configuration that minimizes the exchange energy between the Co moments across the oxidation interface is an antiparallel state of the net magnetization [Fig. 1(c)]. At the same time, the dipolar energy is reduced since the net magnetization of the left-hand and right-hand regions form a flux-closure configuration. A sufficiently high external magnetic field can twist the antiparallel magnetization state to the parallel state [Fig. 1(d)], so reducing the Zeeman energy [26,27,30,36,39]. This switching process is accompanied by the creation of a domain wall (DW) for the Co and Gd moments associated with an energy cost E_{DW} . In the regime where the dipolar energy is negligible (see Supplemental Material [37]), the DW energy determines the strength of the effective antiparallel coupling J_{AP} between the net magnetization in the regions with compensation temperatures of T_{c1} and T_{c2} . The antiparallel coupling gives rise to an effective exchange coupling field H_{EC} :

$$\mu_0 H_{\text{EC}} = \frac{J_{\text{AP}}}{M_{\text{net}}} \cong \frac{\lambda_{\text{DW}}}{M_{\text{net}} w} = \frac{4\sqrt{A_{\text{eff}} K_{\text{eff}}} - \pi D}{M_{\text{net}} w}, \quad (1)$$

where λ_{DW} , A_{eff} , K_{eff} , D , M_{net} , and w are the DW energy density, effective exchange stiffness, effective magnetic anisotropy, DMI strength, net magnetization, and the width of the switched area, respectively [37].

The impact of the coupling on \mathbf{M}_{Co} and \mathbf{M}_{net} [illustrated in Fig. 1(c)] can be demonstrated by selectively oxidizing a checkerboard pattern with a square width of 800 nm in a film with $T_M > \text{RT}$, as schematically shown in the inset of Fig. 1(e). After removal of a large magnetic field saturating

the sample, the Kerr contrast, predominantly arising from the Co sublattice, displays a uniform state [Fig. 1(e)]. In contrast, the magnetic force microscopy image, where the stray fields produced by the net magnetization are detected, reveals an alternating contrast [Fig. 1(f)]. The nanoscale magnetization pattern is predominantly driven by lateral exchange coupling whereas increasing the dimensions towards a micrometer scale pattern would lead to an increase in the influence of the dipolar interaction [36]. To further demonstrate this lateral exchange coupling at ambient temperature, we patterned a $50\text{-}\mu\text{m} \times 50\text{-}\mu\text{m}$ square with half of the square being oxidized [light and dark grey regions of the square in Fig. 1(g)]. The as-grown part of the square [white region of the square in Fig. 1(g)] is compensated with T_M slightly above RT, such that its magnetization is negligible. The oxidized region has its T_M far below RT, resulting in a lateral exchange-biased structure. As shown in Fig. 1(g), by warming up from 250 to 300 K in an applied magnetic field $\mu_0 H_z = \pm 6$ T in order to preset the state of the compensated region, a switching of the exchange-biased hysteresis loop ($\mu_0 H_{EB} = \pm 24$ mT) can be observed depending on the state of the compensated region [37].

In order to confirm the interfacial origin of the exchange coupling, we selectively oxidized tracks with widths in the range 50–200 nm in the original GdCo films. The electric detection of the magnetic state (M_{Co}) is performed via 1- μm -wide Hall bars [Fig. 2(a)]. Full and minor hysteresis loops at temperatures ranging from 300 K down to 200 K are then recorded [37]. An example set of hysteresis loops for a 150-nm-wide track measured at 300, 220, and 200 K, corresponding to the three distinct temperature ranges, is presented in Fig. 2(a). As expected, the hysteresis loops in the temperature range with $T > T_{c2}$ [300-K loop in Fig. 2(a)] and $T < T_{c1}$ [200-K loop in Fig. 2(a)] are trivial since the net magnetization of both the T_{c1} and T_{c2} regions simply switch when applying a sufficient magnetic field. In the temperature range $T_{c2} > T > T_{c1}$, on application of a large enough magnetic field, the Zeeman energy will cause the net magnetization of both regions to follow the applied field, leading to M_{Co} in the oxidized and nonoxidized regions pointing in opposite directions. On reducing the magnetic field, the exchange coupling overcomes the Zeeman interaction resulting in parallel orientation of the two Co magnetic sublattices. This is accompanied by an enhancement of the Hall signal [37]. After surpassing the coercive field of the surrounding nonoxidized GdCo layer, the magnetization switches while maintaining the parallel Co magnetic configuration. When the field is further increased, the net magnetization in the two regions again aligns in parallel.

The systematic measurement of the exchange coupling strength at different temperatures is summarized in Fig. 2(b). In line with the proposed mechanism, no exchange coupling field is observed when the temperature is above or below both T_{c1} and T_{c2} . However, once the temperature is below T_M of the surrounding nonoxidized GdCo layer, an increase in the exchange coupling field can be observed as the magnetization of the track approaches its compensation point on reducing the temperature. The increase in the exchange coupling field is caused by the reduction of the net magnetization of the tracks, which can be quantitatively described by Eq. (1) and fitted

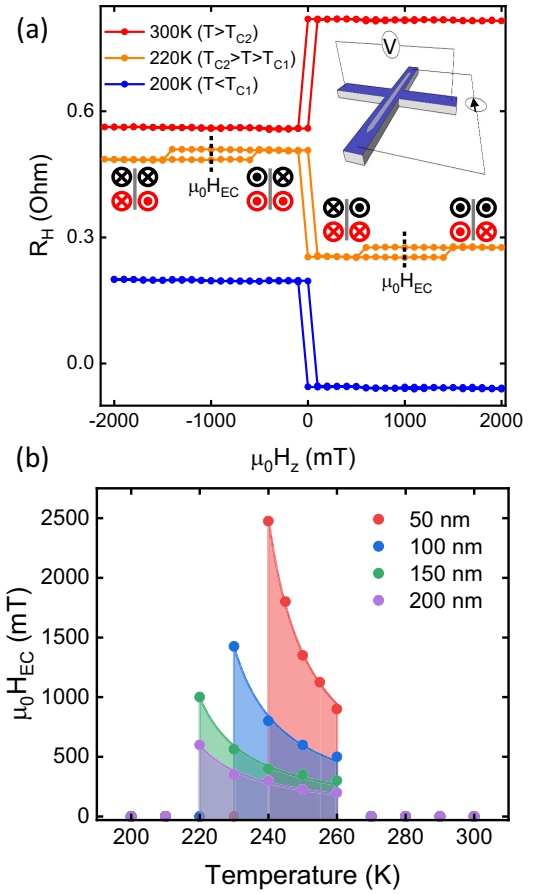


FIG. 2. Temperature dependence of the lateral exchange coupling. (a) A set of hysteresis loops measured via Hall resistance as a function of applied magnetic field of a 150-nm-wide track at different temperatures. The plots are shifted by 0.3 and 0.6 Ohm (for 220 and 300 K) for clarity. In the inset is a schematic of the oxidized track (in gray) on a 1- μm -wide Hall bar (in blue) used for anomalous Hall resistance measurements. The relevant magnetization states of oxidized/nonoxidized regions are depicted (black for M_{net} and red for M_{Co}). (b) Exchange coupling field versus temperature plots for different track widths in the range 50–200 nm. The lines are fits according to Eq. (1). The thickness of the GdCo film is 4.6 nm. Note that the data points outside the shaded regions, where the exchange coupling field is null, overlap.

to the experimental data. By reducing the track width from 200 to 50 nm, the exchange coupling field strength is further increased. This confirms the interfacial origin of the coupling effect, which becomes stronger in devices with reduced lateral dimensions. The exchange coupling fields reach values as high as 2.5 T. It should be noted that, in contrast to the lateral exchange coupling, the dipolar coupling mechanism reported previously [30,36] decreases in smaller devices and is therefore not useful for miniaturization of devices. The micromagnetic simulations of the effective coupling field with and without dipolar field are shown in the Supplemental Material [37] (see, also, Refs. [40,41] therein).

To provide microscopic insight into the switching mechanism, a GdCo film with T_M above RT is patterned into 40- μm -long tracks of various width. Imaging in a wide field polar Kerr microscope reveals that the magnetization

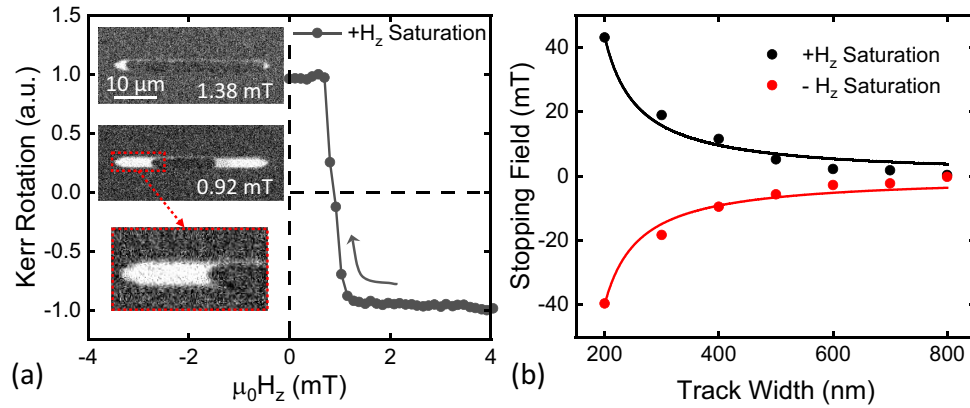


FIG. 3. Determination of the stopping field associated with the lateral exchange coupling. (a) Kerr contrast as a function of decreasing magnetic field obtained from a 2- μm -wide track. The thickness of GdCo is 6.5 nm. Examples of Kerr micrographs at different fields and enlargement of DW profile are displayed in the inset. (b) Stopping field versus track width in GdCo patterned by oxidation. The lines in (b) are fits according to Eq. (1).

reversal is driven by DW propagation along the track [Fig. 3(a)]. The reverse domains [given by white contrast in Fig. 3(a)] are created at the sharp tips at both ends of the track and propagate towards the center. Moreover, the curvature of the moving DWs suggests that the DW is strongly dragged by the lateral interface. The curvature angle of the DW with respect to the DW moving direction is in stark contrast to the case where the DW motion is hindered by pinning at the edges of a magnetic racetrack [42]. The DW can then serve as a probe of the magnetic coupling [18]. We measure the so-called stopping field at which the DW motion is arrested, meaning that the exchange coupling is balanced by the Zeeman energy. The stopping field can be deduced from the hysteresis loop, an example of which is shown in Fig. 3(a), and corresponds to the field value where the Kerr rotation switches sign. A clear increase of the stopping field is observed when the track width is reduced from 800 to 200 nm [Fig. 3(b)], which again indicates the interfacial origin of the coupling. In addition, the stopping fields are more than one order of magnitude higher than the ones originating from the DMI-driven chiral coupling mechanism, which opens routes to more efficient, tunable lateral couplings [18].

In addition to using oxidation, we can realize lateral exchange coupling using He^+ irradiation, where the spatial modification of T_M is achieved by introducing defects and oxygen atoms into the film [30,31,36,43]. The He^+ irradiation technique offers a good alternative to patterning using oxidation, with exquisite control over the desired coupling strength by changing the irradiation dose and a smaller achievable feature size of 5 nm [44] (see Supplemental Material [37] for the relevant experimental results).

To illustrate the potential of the lateral coupling in a single ferrimagnetic film for applications, we designed a planar counterpart of exchange-biased ferromagnet/antiferromagnet bilayers, in which the exchange bias is manipulated via the spin-orbit torques (SOTs) [45]. We have patterned a compensated GdCo film ($T_M \geq \text{RT}$) into crosslike structures placed on a Pt conduit. The Pt layer is used as a source of sizeable DMI as well of spin current [3,19]. Each cross is divided into five squares, where the four surrounding squares are selectively

oxidized, whereas the central square remains in its pristine state [Fig. 4(a)]. By applying a large (± 250 mT) OOP magnetic field, only the oxidized regions can be switched since they have a sizeable net magnetization [Fig. 4(c)]. In order to utilize SOTs to switch the magnetization, an IP external magnetic field (H) is applied along the current direction (J) [3]. Starting from the case where \mathbf{M}_{Co} is parallel across the entire device, a series of current pulses causes the magnetization in the entire structure to be switched [Fig. 4(d)]. This is caused by the SOT-driven switching of the uncompensated squares, and the central square switches with them due to the strong lateral exchange coupling. From the hysteresis loop in Fig. 4(g), we then see a clear exchange bias field of ± 30 mT whose polarity depends on the orientation of the compensated square set by the SOT. The electric switching of lateral exchange bias is highly reproducible (see Supplemental Material [37]). The unique combination of SOT switching and lateral exchange coupling therefore provides a means to achieve magnetic states, which are otherwise only accessible via a field cooling protocol [Fig. 1(g)]. To corroborate the proposed mechanism, we have also fabricated a complementary cross structure where an oxidized square is placed in the center of the cross while the outer four squares are nonoxidized [Fig. 4(b)]. While a large magnetic field can be used to switch the magnetization of the inner square only [Fig. 4(e)], the SOT is not able to induce switching of the central region because the lateral exchange coupling to the surrounding regions is too strong [Fig. 4(f)].

In conclusion, the lateral exchange coupling reported in single-layer ferrimagnetic devices with submicron dimensions provides an important addition to the family of intralayer couplings. Unlike in vertical stacks, where the interfacial exchange coupling always contains an immobile compensation wall [25–29], the lateral interfacial exchange coupling strength can be easily tuned by modifying the device geometry, altering the He^+ irradiation dose, changing the oxidation exposure, or changing the temperature. The coupling is given by the local exchange interaction between the transition metal atoms across the interface between regions with different compensation temperatures, which allows for

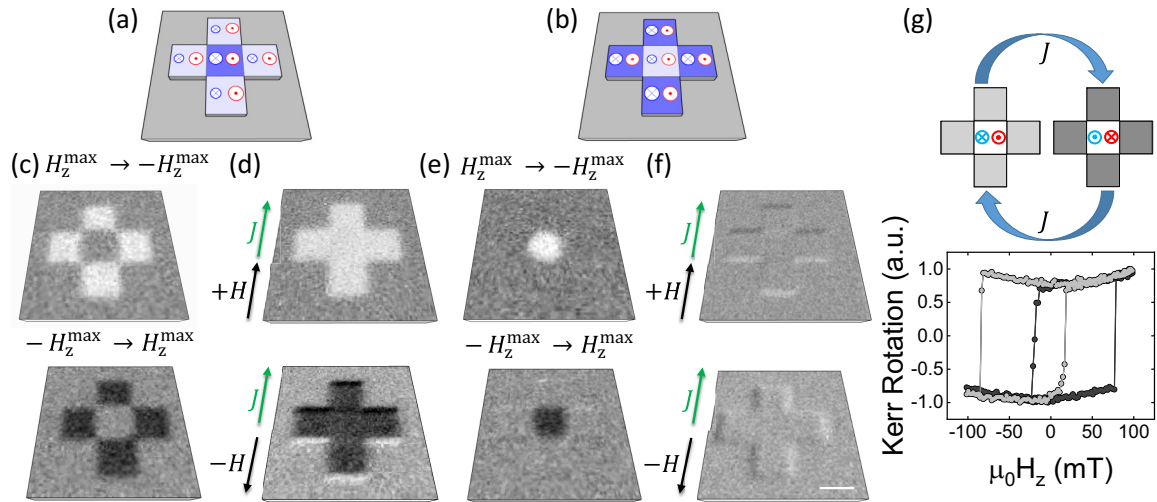


FIG. 4. Electric control of lateral exchange bias. (a),(b) Schematic of a cross structure divided into four oxidized squares surrounding a central compensated square (a) and vice versa (b). The symbols depict the magnetization of the Co (red) and Gd (blue) sublattices, respectively. (c),(e) Kerr differential images after applying a ± 250 -mT OOP magnetic field. (d),(f) Kerr images after applying 100×50 -ns current pulses at $J = 1.35 \times 10^{11}$ A/m², showing that the entire cross has switched from its initial state (d) and no switching (f). An in-plane magnetic field of $H = \pm 200$ mT is applied along the current direction. (g) Hysteresis loops of the four outer squares depicted in (a) for the two magnetic orientations of the compensated central square, $M(\text{Co}) = \odot$ (light gray) and $M(\text{Co}) = \otimes$ (dark gray). The scale bar is 2 μm .

device downscaling without the loss of the coupling strength. The estimated strength of the lateral interfacial exchange coupling is much larger than the volumelike dipolar coupling in ferrimagnetic multilayers [30,36] and it is one order of magnitude stronger than the DMI-mediated coupling in single-layer ferromagnets [16,18]. Furthermore, by combining the interfacial exchange coupling with current driven SOT switching, we are able to access both magnetization states of a compensated ferrimagnet, which can be otherwise only be accessed by a field-cooling protocol. The lateral exchange coupling, where the coupling strength is maintained on downscaling of the device, serves as an important counterpart to the coupling in vertical devices and opens up the possibility for new functionalities in planar devices.

The data that support this study are available via the Zenodo repository [46].

This project received funding from the Swiss National Science Foundation (Grant Agreements No. 200021_182013 and No. 200020_200465). A.H. was funded by the European Union's Horizon 2020 Research and Innovation Program under Marie Skłodowska-Curie Grant Agreement No. 794207 (ASIQS). Z.L. and L.J.H. acknowledge funding from the European Union's Horizon 2020 FET-Open program under Grant Agreement No. 861618 (SpinEngine). Z.L. also acknowledges funding from the National Natural Science Foundation of China (Grant No. 52271160). We thank M. Doebeli for help with the analysis of the ERDA measurements.

-
- [1] C. Chappert, A. Fert, and F. N. Van Dau, in *Nanoscience And Technology: A Collection of Reviews from Nature Journals* (World Scientific, Singapore, 2010), pp. 147–157.
- [2] S. Parkin and S.-H. Yang, Memory on the racetrack, *Nat. Nanotechnol.* **10**, 195 (2015).
- [3] A. Manchon, J. Železný, I. M. Miron, T. Jungwirth, J. Sinova, A. Thiaville, K. Garello, and P. Gambardella, Current-induced spin-orbit torques in ferromagnetic and antiferromagnetic systems, *Rev. Mod. Phys.* **91**, 035004 (2019).
- [4] P. Grünberg, R. Schreiber, Y. Pang, M. Brodsky, and H. Sowers, Layered Magnetic Structures: Evidence for Antiferromagnetic Coupling of Fe Layers Across Cr Interlayers, *Phys. Rev. Lett.* **57**, 2442 (1986).
- [5] S. Parkin, R. Bhadra, and K. Roche, Oscillatory Magnetic Exchange Coupling Through Thin Copper Layers, *Phys. Rev. Lett.* **66**, 2152 (1991).
- [6] J. Nogués and I. K. Schuller, Exchange bias, *J. Magn. Mater.* **192**, 203 (1999).
- [7] R. Stamps, Mechanisms for exchange bias, *J. Phys. D: Appl. Phys.* **33**, R247 (2000).
- [8] E. Hill, S. Tomlinson, and J. Li, The role of dipole coupling in multilayers, *J. Appl. Phys.* **73**, 5978 (1993).
- [9] R. V. Chopdekar, B. Li, T. A. Wynn, M. S. Lee, Y. Jia, Z. Liu, M. D. Biegalski, S. T. Retterer, A. T. Young, and A. Scholl, Nanostructured complex oxides as a route towards thermal behavior in artificial spin ice systems, *Phys. Rev. Mater.* **1**, 024401 (2017).
- [10] D. Y. Sasaki, R. V. Chopdekar, S. T. Retterer, D. Y. Jiang, J. K. Mason, M. S. Lee, and Y. Takamura, Formation of Complex Spin Textures in Thermally Demagnetized $\text{La}_{0.7}\text{Sr}_{0.3}\text{MnO}_3$ Artificial-Spin-Ice Structures, *Phys. Rev. Appl.* **17**, 064057 (2022).

- [11] E. E. Fullerton, J. Jiang, and S. Bader, Hard/soft magnetic heterostructures: Model exchange-spring magnets, *J. Magn. Magn. Mater.* **200**, 392 (1999).
- [12] D.-S. Han, K. Lee, J.-P. Hanke, Y. Mokrousov, K.-W. Kim, W. Yoo, Y. L. Van Hees, T.-W. Kim, R. Lavrijsen, and C.-Y. You, Long-range chiral exchange interaction in synthetic antiferromagnets, *Nat. Mater.* **18**, 703 (2019).
- [13] A. Fernández-Pacheco, E. Vedmedenko, F. Ummelen, R. Mansell, D. Petit, and R. P. Cowburn, Symmetry-breaking interlayer Dzyaloshinskii–Moriya interactions in synthetic antiferromagnets, *Nat. Mater.* **18**, 679 (2019).
- [14] C. O. Avci, C.-H. Lambert, G. Sala, and P. Gambardella, Chiral Coupling Between Magnetic Layers With Orthogonal Magnetization, *Phys. Rev. Lett.* **127**, 167202 (2021).
- [15] S. H. Skjærvø, C. H. Marrows, R. L. Stamps, and L. J. Heyderman, Advances in artificial spin ice, *Nat. Rev. Phys.* **2**, 13 (2020).
- [16] Z. Luo, T. P. Dao, A. Hrabec, J. Vijayakumar, A. Kleibert, M. Baumgartner, E. Kirk, J. Cui, T. Savchenko, and G. Krishnaswamy, Chirally coupled nanomagnets, *Science* **363**, 1435 (2019).
- [17] A. Hrabec, Z. Luo, L. J. Heyderman, and P. Gambardella, Synthetic chiral magnets promoted by the Dzyaloshinskii–Moriya interaction, *Appl. Phys. Lett.* **117**, 130503 (2020).
- [18] Z. Liu, Z. Luo, S. Rohart, L. J. Heyderman, P. Gambardella, and A. Hrabec, Engineering of Intrinsic Chiral Torques in Magnetic Thin Films Based on the Dzyaloshinskii–Moriya Interaction, *Phys. Rev. Appl.* **16**, 054049 (2021).
- [19] Z. Luo, A. Hrabec, T. P. Dao, G. Sala, S. Finizio, J. Feng, S. Mayr, J. Raabe, P. Gambardella, and L. J. Heyderman, Current-driven magnetic domain-wall logic, *Nature (London)* **579**, 214 (2020).
- [20] Z. Luo, S. Schären, A. Hrabec, T. P. Dao, G. Sala, S. Finizio, J. Feng, S. Mayr, J. Raabe, and P. Gambardella, Field-and Current-Driven Magnetic Domain-Wall Inverter and Diode, *Phys. Rev. Appl.* **15**, 034077 (2021).
- [21] Z. Zeng, Z. Luo, L. J. Heyderman, J.-V. Kim, and A. Hrabec, Synchronization of chiral vortex nano-oscillators, *Appl. Phys. Lett.* **118**, 222405 (2021).
- [22] T. P. Dao, M. Müller, Z. Luo, M. Baumgartner, A. Hrabec, L. J. Heyderman, and P. Gambardella, Chiral domain wall injector driven by spin–orbit torques, *Nano Lett.* **19**, 5930 (2019).
- [23] F. Ummelen, H. Swagten, and B. Koopmans, Racetrack memory based on in-plane-field controlled domain-wall pinning, *Sci. Rep.* **7**, 1 (2017).
- [24] A. Belabbes, G. Bihlmayer, F. Bechstedt, S. Blügel, and A. Manchon, Hund’s Rule-Driven Dzyaloshinskii–Moriya Interaction At $3d$ – $5d$ Interfaces, *Phys. Rev. Lett.* **117**, 247202 (2016).
- [25] B. Hebler, P. Reinhardt, G. Katona, O. Hellwig, and M. Albrecht, Double exchange bias in ferrimagnetic heterostructures, *Phys. Rev. B* **95**, 104410 (2017).
- [26] P. Hansen, New type of compensation wall in ferrimagnetic double layers, *Appl. Phys. Lett.* **55**, 200 (1989).
- [27] T. Kobayashi, H. Tsuji, S. Tsunashima, and S. Uchiyama, Magnetization process of exchange-coupled ferrimagnetic double-layered films, *Jpn. J. Appl. Phys.* **20**, 2089 (1981).
- [28] C. Blanco-Roldán, Y. Choi, C. Quiros, S. Valvidares, R. Zarate, M. Vélez, J. Alameda, D. Haskel, and J. I. Martin, Tuning interfacial domain walls in GdCo/Gd/GdCo’ spring magnets, *Phys. Rev. B* **92**, 224433 (2015).
- [29] F. Stobiecki, T. Atmono, S. Becker, H. Rohrmann, and K. Röhl, Investigation of interface wall energy σ_w and coercivity HC in exchange-coupled double layers (ECDLs), *J. Magn. Magn. Mater.* **148**, 497 (1995).
- [30] Ł. Frąckowiak, F. Stobiecki, G. D. Chaves-O’Flynn, M. Urbaniak, M. Schmidt, M. Matczak, A. Maziewski, M. Reginka, A. Ehresmann, and P. Kuświk, Subsystem domination influence on magnetization reversal in designed magnetic patterns in ferrimagnetic Tb/Co multilayers, *Sci. Rep.* **11**, 1041 (2021).
- [31] M. Krupinski, J. Hintermayr, P. Sobieszczyk, and M. Albrecht, Control of magnetic properties in ferrimagnetic GdFe and TbFe thin films by He⁺ and Ne⁺ irradiation, *Phys. Rev. Mater.* **5**, 024405 (2021).
- [32] K. Buschow, Intermetallic compounds of rare-earth and 3d transition metals, *Rep. Prog. Phys.* **40**, 1179 (1977).
- [33] D.-H. Kim, M. Haruta, H.-W. Ko, G. Go, H.-J. Park, T. Nishimura, D.-Y. Kim, T. Okuno, Y. Hirata, and Y. Futakawa, Bulk Dzyaloshinskii–Moriya interaction in amorphous ferrimagnetic alloys, *Nat. Mater.* **18**, 685 (2019).
- [34] M. Huang, M. U. Hasan, K. Klyukin, D. Zhang, D. Lyu, P. Gargiani, M. Valvidares, S. Sheffels, A. Churikova, and F. Büttner, Voltage control of ferrimagnetic order and voltage-assisted writing of ferrimagnetic spin textures, *Nat. Nanotechnol.* **16**, 981 (2021).
- [35] E. Kirk, C. Bull, S. Finizio, H. Sepelri-Amin, S. Wintz, A. K. Suszka, N. S. Bingham, P. Warnicke, K. Hono, and P. Nutter, Anisotropy-induced spin reorientation in chemically modulated amorphous ferrimagnetic films, *Phys. Rev. Mater.* **4**, 074403 (2020).
- [36] Ł. Frąckowiak, P. Kuświk, G. D. Chaves-O’Flynn, M. Urbaniak, M. Matczak, P. P. Michałowski, A. Maziewski, M. Reginka, A. Ehresmann, and F. Stobiecki, Magnetic Domains Without Domain Walls: A Unique Effect of He⁺ Ion Bombardment in Ferrimagnetic Tb/Co Films, *Phys. Rev. Lett.* **124**, 047203 (2020).
- [37] See Supplemental Material at <http://link.aps.org/supplemental/10.1103/PhysRevB.107.L100412> for additional information of sample fabrication, sample thickness and oxidation dependence, transport measurement, Hall measurement, FIB irradiation, and micromagnetic simulation details.
- [38] R. Malmhäll and T. Chen, Thickness dependence of magnetic hysteretic properties of rf-sputtered amorphous Tb–Fe alloy thin films, *J. Appl. Phys.* **53**, 7843 (1982).
- [39] A. Hrabec, N. Nam, S. Pizzini, and L. Ranno, Magnetization reversal in composition-controlled Gd_{1-x}Co_x ferrimagnetic films close to compensation composition, *Appl. Phys. Lett.* **99**, 052507 (2011).
- [40] A. Vansteenkiste, J. Leliaert, M. Dvornik, M. Helsen, F. Garcia-Sanchez, and B. Van Waeyenberge, The design and verification of MuMax3, *AIP Adv.* **4**, 107133 (2014).
- [41] L. Caretta, M. Mann, F. Büttner, K. Ueda, B. Pfau, C. M. Günther, P. Helsing, A. Churikova, C. Klose, and M. Schneider, Fast current-driven domain walls and small skyrmions in a compensated ferrimagnet, *Nat. Nanotechnol.* **13**, 1154 (2018).
- [42] L. Herrera Diez, F. Ummelen, V. Jeudy, G. Durin, L. Lopez-Diaz, R. Diaz-Pardo, A. Casiraghi, G. Agnus, D. Bouville, and

- J. Langer, Magnetic domain wall curvature induced by wire edge pinning, *Appl. Phys. Lett.* **117**, 062406 (2020).
- [43] A. Krasheninnikov and K. Nordlund, Ion and electron irradiation-induced effects in nanostructured materials, *J. Appl. Phys.* **107**, 071301 (2010).
- [44] I. Shorubalko, K. Choi, M. Stiefel, and H. G. Park, Ion beam profiling from the interaction with a freestanding 2D layer, *Beilstein J. Nanotechnol.* **8**, 682 (2017).
- [45] P.-H. Lin, B.-Y. Yang, M.-H. Tsai, P.-C. Chen, K.-F. Huang, H.-H. Lin, and C.-H. Lai, Manipulating exchange bias by spin-orbit torque, *Nat. Mater.* **18**, 335 (2019).
- [46] Z. Liu, Z. Luo, I. Shorubalko, C. Vockenhuber, L. J. Heyderman, P. Gambardella, and A. Hrabec, Dataset for Strong lateral exchange coupling and current-induced switching in single-layer ferrimagnetic films with patterned compensation temperature, Zenodo, [10.5281/zenodo.6936908](https://doi.org/10.5281/zenodo.6936908).